ABSTRACT

Title of Thesis: DEVELOPMENT OF HIGH THROUGHPUT
                         POLARIZATION MAINTAINING NSOM PROBES

                         Vivekananda P. Adiga, M.S., 2005

Directed By: Associate Professor Raymond Phaneuf,
                         Department of Materials Science and Engineering

                         Professor H. Dennis Drew,
                         Department of Physics

High throughput, polarization maintaining probes for Near-field Scanning Optical Microscopy (NSOM) were fabricated by chemical etching. An aperture was formed with Focused Ion Beam after coating the tips with 300 nm of aluminum. Tips showed a typical far field polarization extinction ratio of 100 to 1. The throughput of the tips depends on the polarization of the incident light because of the boundary conditions imposed by elliptical aperture.

 We show NSOM images obtained with these probes on gold dots on a GaAs substrate. NSOM images show a contrast inversion on the gold dots compared to the far-field imaging. We were not able to determine the spatial resolution of the probes since the topographic effects dominate the optical response. Interference effects and variation of the light intensity in close proximity to the sample are observed and studied.

DEVELOPMENT OF HIGH THROUGHPUT
POLARIZATION MAINTAINING
NSOM PROBES

By

Vivekananda Parampalli Adiga

Thesis submitted to the Faculty of the Graduate School of the
University of Maryland, College Park, in partial fulfillment
of the requirements for the degree of
Master of Science
2005

Advisory Committee:
Associate Professor Raymond Phaneuf, Chair
Professor Dennis Drew
Associate Professor Ichiro Takeuchi

Dedication

To my parents

Acknowledgements

I would like to thank my advisor Prof. Dennis Drew for his help whenever I had problems in the lab. I would greatly appreciate his patience and time in completing this thesis.

I would greatly appreciate my lab members Paul Kolb, Don Schmadel, Geoff Evans, Max Cubillos, Ben Palmer for their assistance during the course of this research. I would also like to thank Prof. Ray Phaneuf for his support and providing the samples for NSOM scans.

Other people to whom I am indebted for being very valuable to me with my life and work are my brother Shashi, my sisters renuka, mallika and my parents.

Thank you everyone for being so kind and helpful to me.

Table of Contents

List of Figures

1. Introduction

In 1928 Synge [1] proposed a technique to overcome the diffraction limit of classical optical microscopy. He proposed the idea of forcing the light through a sub wavelength aperture and raster scanning it in the close proximity ($d<\lambda/2$) to the sample and it was demonstrated for microwaves by Ash and Nicols [2]. In 1984 Pohl et al [3] demonstrated a near-field optical imaging system based on metal-coated etched quartz tips to form the aperture. Later the instrument was called as a Near-field Scanning Optical Microscope (NSOM) in US or Scanning Near-field Optical Microscope (SNOM) in Europe. NSOM typically uses a sub wavelength aperture surrounded by a metallic coating which helps to confine the electromagnetic fields and is scanned in close proximity to the sample. Betzig and Trautman [4] made a major improvement on Pohl et al's scheme by tapering the optical fiber to form probe. The tapering was done by mechanically pulling the fiber while locally heating it with CO_2 laser. The aperture was formed by coating the pulled tip at an angle to avoid covering the end face. This technique increased the signal strength and resolution.

A further increase in the resolution and the throughput of the NSOM was achieved by etching the optical fibers [5, 6, 7]. Etching not only gave the tips with apertures as small as 10nm, the throughput of the tips was increased by a factor of at least 1000. This drastic improvement in the throughput coupled with resolution improved the ability of NSOM to conduct experiments such as Raman scattering [8, 9], fluorescence imaging of single molecules [10], and photoluminescence measurements to image Quantum Dots [11]. Along with the improvements in the

resolution and throughput, there were advances in techniques to control the tip-sample separation. This distance is controlled by shear force feedback mechanism which relies on the interaction of the tip with the sample in close proximities (~30nm) [12]. This is done by gluing the fiber probe to a tuning fork and recording the damping in its oscillations in close proximity to samples. Light emitted or collected by the NSOM probe is used to determine the optical properties such as transmittance, reflectance, florescence, or photoluminescence of the material. Surface topographic image are simultaneously obtained and facilitates the interpretation of the data.

There are many factors which influence the contrast during the NSOM imaging such as tip-sample separation, collection optics [13] and polarization of the illumination. Polarization of the light from the tip greatly affects the contrast [13]. In the reflection mode NSOM, this contrast could be due to the position of the detector [14] or the polarization dependent optical response of the sample [15]. In transmission NSOM the polarization of the illumination strongly affects the contrast especially when imaging submicron metallic objects [16, 17]. Orientation of the molecular dipole can be determined in single molecule fluorescence imaging if the polarization of the incident light is known [18]. Magnetic domains in magneto-optic materials can be read using a light of known linear polarization [19]. However it is very difficult to control the polarization of the light inside a conventional circular core fiber waveguide since the phase of polarization state are can be easily changed at the bends, stressed portions of the fiber or at non uniform cross section of the circular core of the fiber [20]. Apart from these effects, external perturbations such as changes in temperature or position will change polarization of the output beam as a function of

time. Commercially available 3-paddle polarization manipulators are generally used to control the polarization. But the axis and amount of rotation of the polarization can not be known [15]. It is desired to know the polarization coming out of the NSOM probes which will greatly help in interpreting the data. It will also enable us to carefully illuminate a selective polarization to the sample.

This can be achieved by using polarization maintaining (PM) single mode fibers. Polarization maintaining fiber preserves the input polarization by separating the propagation constants of two fundamental modes. Light polarized along one axis of the fiber travels at a different rate than the light polarized orthogonal to that axis. These two principle transmission axes are called as fast and slow axes. A linearly polarized light input into a PM fiber along one of these principle axes will give a linearly polarized output. This is done by inducing a strong, permanent, internal birefringence in the fiber such that birefringence effects due to external perturbations are negligible compared to the internal birefringence. Such a birefringence can be induced in the fibers by making the fiber core in elliptical shape [21, 22] or by incorporating stressed regions surrounding the core [23,24, 25]. Most of the PM fibers like "panda" or "bow-tie" fibers have stress-induced birefringence. Due to the nature of the regions and stress inside these fibers they can not be etched to form probes. Mitsui, T. and Sekiguchi, T. [26] have recently reported probes made from polarization maintaining panda fibers by mechanically pulling them. But they faced the same problems associated with pulling such as a lower throughput, and a very low polarization extinction ratio. I have developed the probes from elliptical core polarization maintaining fibers by chemical etching. In these fibers the birefringence

3

is primarily introduced by geometry. Birefringence increases with core ellipticity and with the square of core-cladding index difference but fiber attenuation generally increases with the increase in ellipticity [27].

The organization of the thesis is as follows: Chapter 2 describes the fabrication of the probes; Chapter 3 covers the characterization of the probes such as polarization maintenance and throughput. Chapter 4 gives the preliminary NSOM images obtained with these probes.

2. Fabrication of the Probes

2.1 Elliptical Core Fiber specifications

The fiber* we used has GeO_2 doped 2 μm by 1 μm elliptical core. Fiber has an attenuation of 12 db/ km for λ=630nm. To reduce the interference effects caused by light that is launched or strays into the cladding, the refractive index of the cladding surrounding the core is made below that of the surrounding medium. This non guiding cladding rapidly attenuates the light launched into it. A high index difference minimizes the effect of radiation around the small radius of curvature and also helps the manufacturers to increase the size of the core required for single mode operation of the fiber [27, 28]. The elliptical core fiber has three different regions, GeO_2 doped silica core (n=1.453), fluorine doped cladding surrounded by pure silica region as in the Fig. 2.1 The core-inner cladding index difference is Δn=0.035, the inner cladding index is depressed below that of surrounding outer silica cladding by Δn_c =0.003. The fiber has a UV cured acrylate jacket, which has an index higher than the silica cladding. The fiber has a typical polarization extinction ratio of about 20. Due to the manufacturing process the center of the core has pure silica region with a diameter of about 50nm [27], it has to be made homogeneous to fabricate the probes.

*   Fiber source KVH industries

5
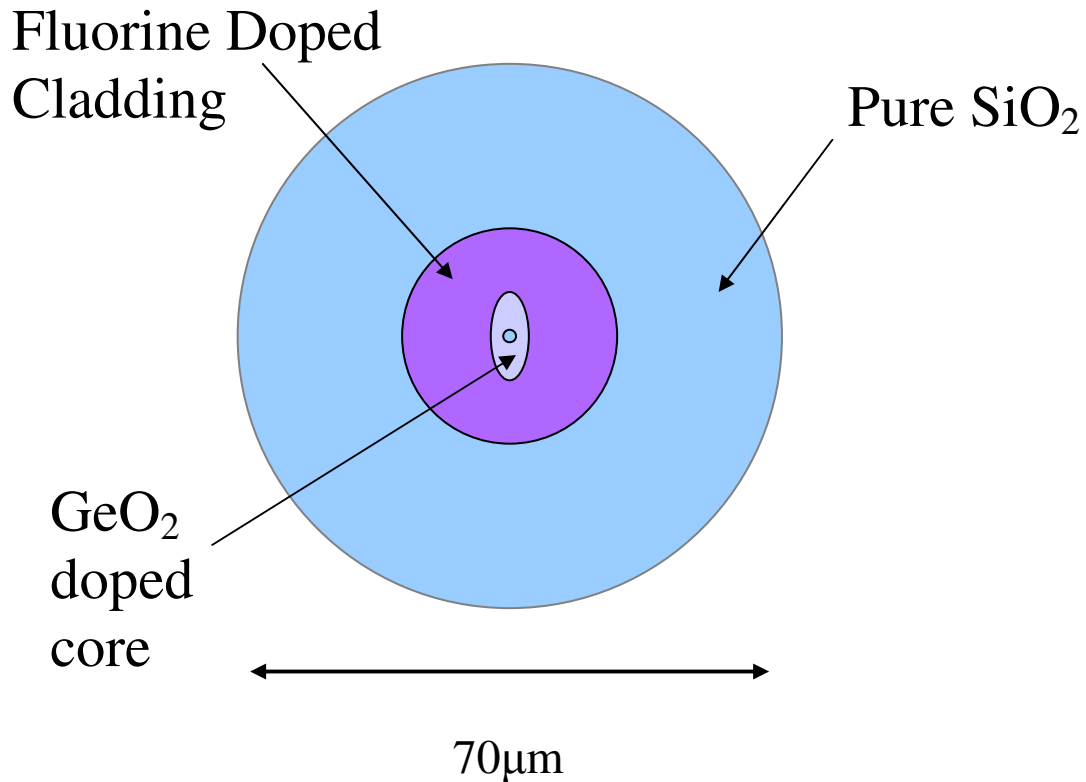
Figure 2.1: Cross section of the elliptical core fiber. It has an overall diameter of about 70 μm. The fluorine doped silica cladding has a diameter of about 10 μm. The central GeO_2 doped core has a major axis of 2 μm and minor axis of 1 μm. Central blue region is the under doped core

2.2 Fabrication steps

2.2.1 Heating the Fiber

To get sharp tips the core has to be homogeneous; initially it is not, but can be made so by heating the fiber. Before heating the fiber it is stripped out of its jacket at the very end using a razor blade. The fiber is cleaned with acetone and cleaved using a York FK 11 Fiber Cleaver. An optical microscope is used to check for the flatness of

the end surface. Heating temperature has to be selected in such a way that the dopant diffusion takes place in the minimum possible time without changing the shape of the fiber. Too low temperature takes more time for the complete diffusion and causes a reduction in the strength of the fiber. Over heating results in diffusion of the GeO_2 into the fluorine doped cladding. I found that the optimum temperature for diffusion is approximately 1650˚C. Fibers heated in air resulted in uneven surfaces as in figure 2.3b which reduced their strength compared to the fibers heated at vacuum. To prevent this fibers are heated in tantalum boats for 2 minutes in a vacuum chamber. Since this temperature is above glass transition, fibers have to be mounted vertically during heating to avoid bending.
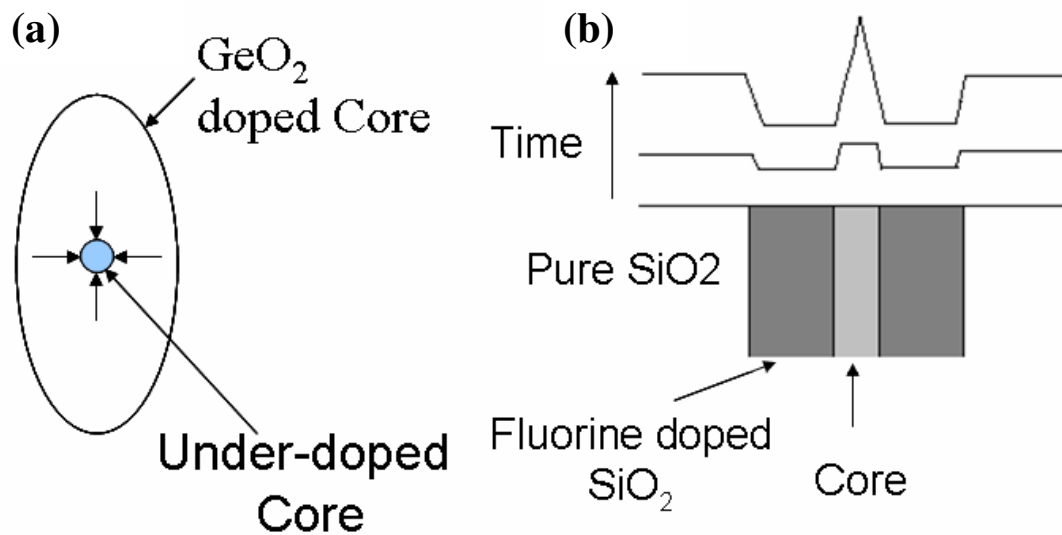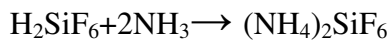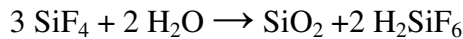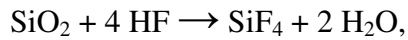

Figure 2.2 (a) Schematic of diffusion process. (b) Schematic illustration of selective chemical etching of the cleaved fiber. Very end of the tip has an elliptical shape.

2.2.2 Selective chemical etching

The selective chemical etching technique I used is based on the difference in the etching rates of different regions of the fiber in Buffered Oxide Etchant (BOE) [29]. BOE consists of mixture of NH_4F (40%) solution and HF (49%) solution in ratio of x:1 respectively. Etching characteristics of different regions of the fiber depends on this ratio. For lower values of x (x<5) the GeO_2 doped core etches at faster rate compared to fluorine doped silica cladding and pure silica cladding. As the concentration of the HF in the mixture decreases (x>5) GeO_2 doped core etches at a slower rate and it protrudes out and forms a sharp tip as the etching continues as shown in figure 2.2b. The fluorine doped silica region etches at a faster rate than the GeO_2 doped core and pure silica cladding and the rate is independent of the proportion of the constituents of the etchant [29].

The chemical reactions which occur during the etching are [30, 7]

$$SiO_2 + 4\ HF \longrightarrow SiF_4 + 2\ H_2O,$$

$$3\ SiF_4 + 2\ H_2O \longrightarrow SiO_2 + 2\ H_2SiF_6$$

$$H_2SiF_6 + 2NH_3 \longrightarrow (NH_4)_2SiF_6$$

Similarly, GeO_2 undergoes analogous reactions, but H_2GeF_6 dissolves at a different rate compared to H_2SiF_6, which is responsible for the slower or faster etching of the GeO_2 doped region [7] depending on the proportion of the constituents of etching. The cone angle and sharpness of the tips can be controlled by varying concentration

of the etching solutions and the temperature [30]. Fibers were etched in 30:1 (30 parts of NH_4F solution and 1 part of HF solution by volume) solution at room temperature, since this solution gives the sharp tip with smooth surfaces after etching for 3 hours. The etching resulted in a tip, which has a height of about 1.75 µm and is surrounded by a crater formed by the fluorine-doped cladding, which etches at faster rate than the core and pure silica cladding. The apex of the tip has dimensions of about 20 nm by 100 nm. This elliptical shape of tips obtained with this technique gives unique optical transmission properties to the probes which I will discuss later on in this thesis. Fig 2.3a and 2.3b show a SEM image of the cross section of the fiber after selective etching. Fiber in figure 2.3a is heated in vacuum, while fiber in figure 2.3b is heated in open air in silicon carbide furnace at 1550°C. The rough surfaces formed on the outer edges of the fiber heated in air could be because of the rapid cooling, which might have induced stress in the fiber. Figure 2.3c shows higher magnification images of the protruded core obtained from cleaved fibers without heating. Central under doped silica etches at a faster rate, which exposes more surfaces for etching resulting in an inverted cone structure. The heating at 1650°C in vacuum results in homogeneous core which helps to make sharp tips as in Fig 2.3d The fibers were coated with 100nm of gold by sputter deposition before imaging. The ratio of the effective height (Height of the protruded core – Depth of the crater ≈ 0.75 µm) of the tip to the diameter of the fiber (70 µm) is very low. During operation of the NSOM in reflection mode the large cladding would shadow the light. The crater surrounding the tapered core could act like a cavity which makes it difficult to

9

interpret the images obtained from these tips in reflection mode. A tapered probe can be obtained with meniscus etching.
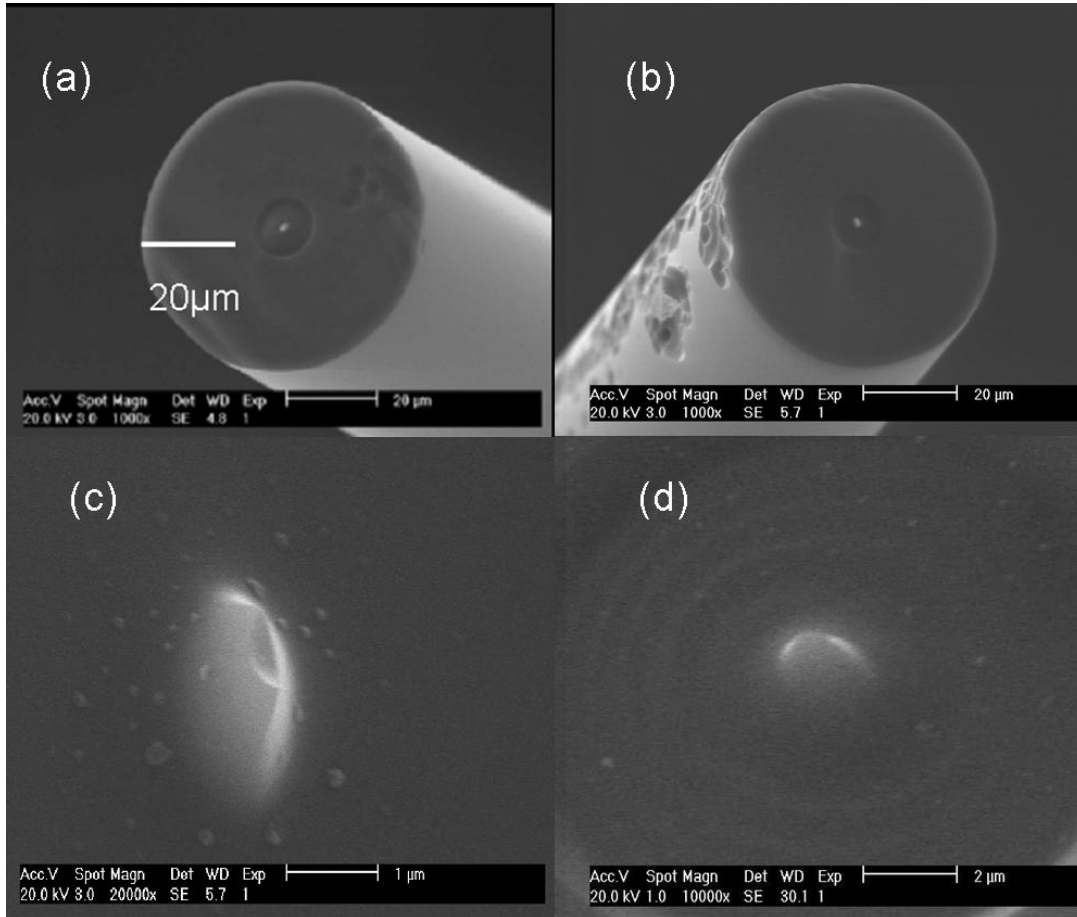

Figure 2.3 SEM images of etched fiber using a 30:1 solution (a) Cross section of fiber heated in vacuum at 1650° C (b) Cross section of fiber heated in air in silicon carbide furnace. (c) Higher magnification image of the core of the etched fiber obtained without heating. (d) Tapered core of the fiber after heating in tantalum boat at 1650 ºC for 2 min and etching in 30:1 solution.

2.2.3 Meniscus etching

Meniscus etching is done by covering the surface of the etchant with a protective layer which is immiscible in the etchant and dipping the cleaved fiber in the etchant. The etchant forms a meniscus at the interface between the fiber and the etchant [6]

The Laplace-Young equation describes the behavior of the meniscus

$$\Delta p_c = \sigma \left(\frac{1}{R_1} + \frac{1}{R_2} \right) \quad (1)$$

Where R_1 is the radius of the fiber, R_2 is the radius of curvature of the "meniscal" surface along a radius from the fiber's axis, ΔP_c is the pressure difference between the protective layer and the etchant

$\Delta P_c = \Delta \rho \times g$ where $\Delta \rho$ is the density difference between the layer and the etchant. σ is the surface tension which keeps the liquid surrounding the fiber above the normal level.

The meniscus has to drop down in order to balance the increased volume of the etchant (due to etching) with surface tension. The meniscus height drops linearly with radius since radius of the fiber is very small compared to the capillary constant [5]. A protective layer of isooctane prevents the evaporation of the etchant and thus maintains the etchant level. It also protects the surrounding equipment from corrosive HF gas. The initial height of the meniscus governs the taper angle and depends on the radius of the fiber, the protective layer used, concentration of the etchant, temperature, and fiber material. A pencil shaped probe obtained by this method has an apex diameter of about 1 micron. The etched surface of the taper are very rough

compared to those produced by selective chemical etching. A rough surface at the very end of the taper greatly affects transmission properties of the coated fiber probe. It also causes the pinholes. In order to reliably obtain apex dimensions at the nano-scale in elliptical shape and also to obtain smooth tips I combined both meniscus and selective chemical etching. I did this as follows. Fibers were etched with 10:1 BOE solution kept in a polystyrene container, which was covered with a plastic cap. The etchant was covered with iso-octane as the protective layer because of its low volatility and miscibility in the etchant. To minimize the vibrations the entire set-up is placed on an air table. The very end of the cleaved fiber is brought down until it just touches the layer-etchant interface which is indicated by the formation of the meniscus.
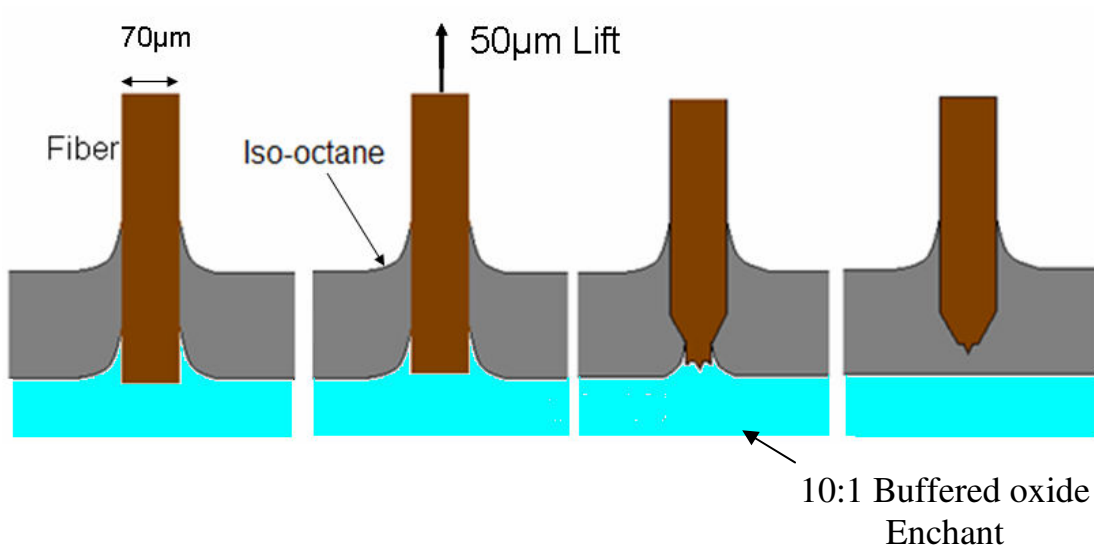

Figure 2.4: Schematic representation of the etching process. The meniscus drops when it reaches the fluorine doped cladding.

The fiber is gradually lifted up by about 50 microns as in fig 2.4. The etching takes about 10 hours and results in a taper length of about 170 microns. The pencil shape is obtained from the meniscus etching and selective chemical etching forms the central tip. The height of the lift (50 µm) is chosen in such a way that meniscus drops from the fiber after it etches pure silica region and just reaches the fluorine doped cladding. Hence by proper adjustment of the height of the lift we can avoid the crater surrounding the core. The boundary of the plateau corresponding to fluorine-doped cladding formed by the etching is not circular as in figure 2.5a The faster etching in those regions could be caused by the stresses in the fiber induced during the manufacturing process. Etching in those regions reaches a much higher rate as fluorine-doped cladding gets exposed to the etchant. A further reduction in the diameter requires great control over the etching. Fibers are etched in 30:1 BOE solution in the final stages of etching since it allows a better control over the shape of the probe. Final plateau has dimensions of about 10 µm by 7 µm. For reflection based NSOM it is better to have a smaller diameter as the plateau tends to shadow the light from the tip.

Tips can also be produced by another method. The cleaved end of the heated fiber is completely immersed in the etchant. The fiber is tapered down until the very end by meniscus etching. Dipping it again in etchant solution sharpens this tip by selective chemical etching. But as in the figure 2.6 the tips made by this process have a long protruded core formed due to the rapid etching of fluorine-doped cladding surrounding the core. Although we have not characterized these tips, they are expected to have very low throughput because of the longer tapered core.
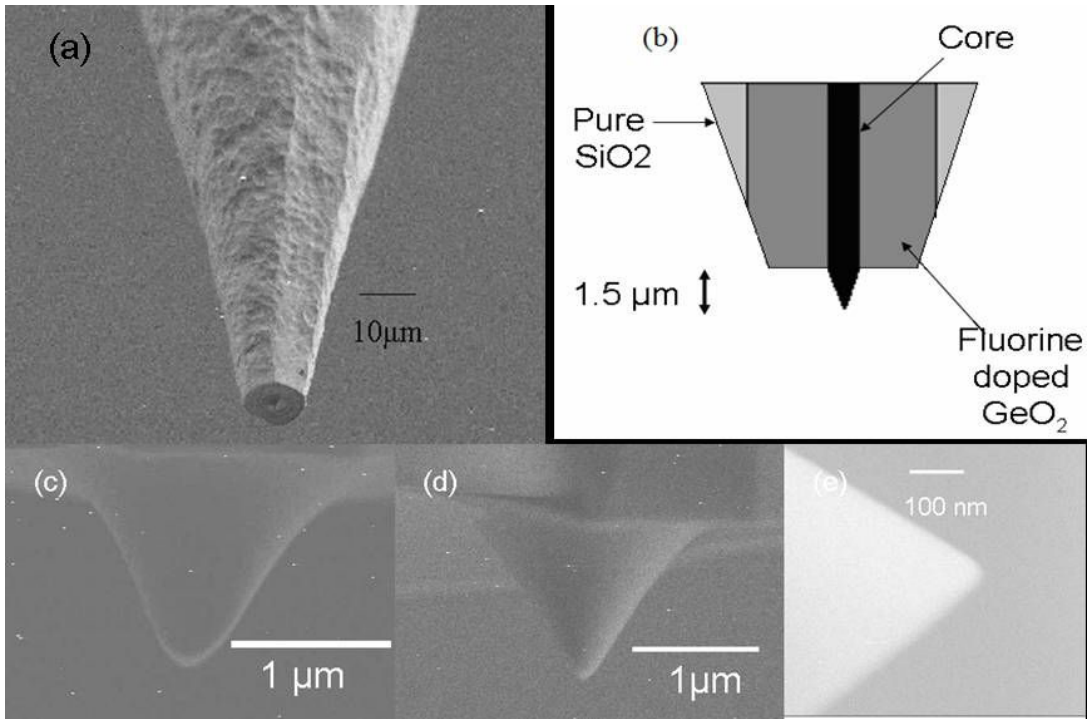
Figure 2.5: (a) SEM image of the tip fabricated with single stage etching process. (b) Schematic of the tip profile. SEM images of the profile of the tapered core along different directions (c), (d) and a high magnification image of the apex of the tip (e).
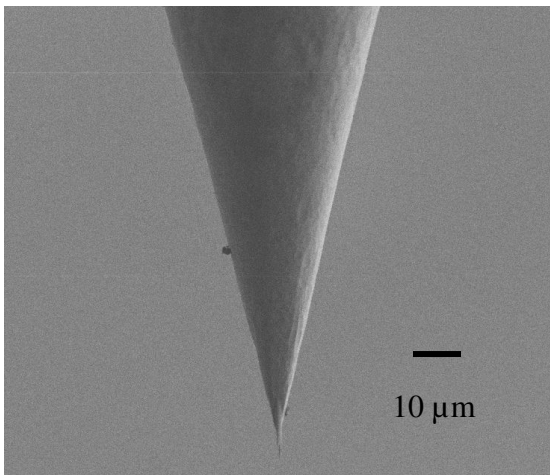

Figure 2.6: SEM image of the fiber obtained after double stage etching process. Core protrudes out by about 10 microns.

2.2.4 Aluminum Deposition

To contain the light we have to coat the tip with a metal film. Aluminum is the preferable metal for this since it has a very high reflectance in the visible region and a small skin depth of about 7nm at λ=635nm. A lower skin depth, besides increasing the resolution by confining the light, decreases the thickness of the coating required which helps to make sharper tips. Conventional mechanically pulled tips which have very low optical transmission efficiencies require at least 100 nm of aluminum to sufficiently attenuate the light transmission through the aluminum coating. A 100nm of coating reduces the transmission of light through the film by a factor of e^{15}. Etched tips require less coating since throughputs are much higher. The fibers are cleaned with boiling piranha etch solution to remove the dust particles, which can cause pinholes after coating. Fibers are coated in a thermal evaporation chamber while rotating them at a constant velocity [31]. The vacuum chamber is pumped down to 10^{-6} Torr using a diffusion pump. Deposition is done using a triple stranded tungsten helical element with six coils. Al staples (99.999%) are hung on the loops of the element. As we heat the element beyond melting temperature of Al it wets the filament to lower its surface tension. The filament is slowly heated, and as the deposition rate of 10 A/s is reached the motor is turned on. After coating the fiber with 300nm of Aluminum the deposition is stopped by turning off the heating current and the fibers are allowed to cool down. A schematic of the set up is shown in figure 2.7. Because of the geometry of our probes, coating may not be uniform on all surfaces. The taper formed by meniscus etching is rough and protrusions may result

in shadowing of some parts during the coating. To avoid these problems the probes are coated with the source at two different angles.
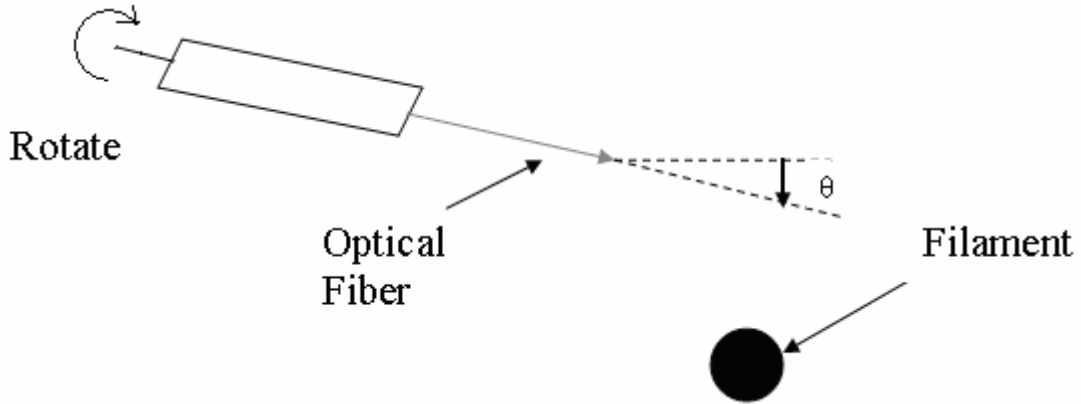

Figure 2.7: Schematic of metallization setup. Etched tips were at about 10 cm from the filament. $\theta \approx -10°$ for the first coating, and $\theta \approx +10°$ for the second coating in which the very end of the tip is turned away.

The first coating coats all the surfaces of the probe. During the second coating very end of the probe is turned away from the filament so that coating takes place only in the taper formed by meniscus etching. The present procedure produces an aluminum coating much thicker than required amount, it might be reduced by calibrating the evaporator.

2.2.5 Aperture fabrication

The aperture is formed by carefully slicing the very end of the coated tip with a focused ion beam (FIB) of gallium [32, 33, 34]. FIB gives an atomically smooth surface; hence we can avoid spurious contrast due to the roughness of the tip during the operation [35]. FIB etching is done at a moderate ion beam density (30KV, 11pA) with focused beam 90° to the probe axis. Fig 2.8 shows a tip fabricated with FIB

having a well defined aperture of 55 ± 5nm by 220 ± 5nm and a flat end face. Different aperture sizes can be fabricated by slicing the tip at different positions. Apertures with minor dimensions ranging from 20 ± 5 nm to 150 ± 5 nm were fabricated using this technique to characterize the tips.
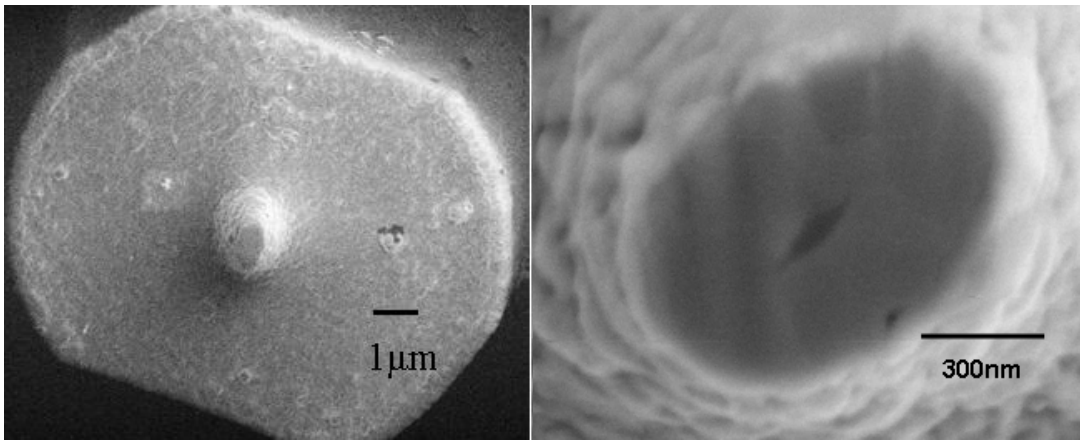

Figure 2.8 Aperture fabricated with FIB. The central dark region is the exposed core.

3. Characterization of the Probes

3.1 Orienting the fiber

To characterize the probes made from the elliptical fiber, we have to know the major and minor axis of the fiber, which can be determined by the following method [27]. A beam of light from a coherent source is made to pass through a hole in a white screen. The beam is projected onto fiber orthogonally to fiber axis. An interference pattern, reflected from elliptical core appears on the screen. When we rotate the fiber the interference fringes change their direction 4 times during the 360-degree rotation. When the fringes are stationary, one of the axes is parallel to the incident beam. The rate of change in the direction of movement of the fringes is used to determine the major and minor axis of the fiber. After we orient the fiber we glue it on to an iron holder, so that the orientation is preserved.

3.2 Polarization Maintenance

To characterize the polarization maintaining property of the probes a polarizer is placed in between the probe and the detector, which are placed approximately 1 cm apart. A Hitachi HL 6320 G laser diode (λ = 635nm) is used to couple the plane polarized light directly into the cleaved fiber. The metallic protective cap of the diode is removed which allows us to place the fibers at a close proximity to the laser. The laser diode is mounted on a rotational mount which allows us to rotate it through 360∘ and its output is modulated with a 1k Hz signal. The oriented fiber is mounted on a micrometer, at about 150 µm from the laser diode, with its minor axis parallel to the electric field. The intensity of the light through the fiber is maximized by adjusting its

18

lateral position using micrometer while keeping the distance between laser diode and fiber constant. The distance between the fiber and the laser is determined by observing the size of the shadow produced by the fiber on a screen placed at 1.75″ from the diode. The distance is also verified using an optical microscope situated right above the fiber and the laser. Figure 3.1 shows the schematic of the light coupling set-up. Before characterizing the probes, they are inspected for pinholes under a microscope with a 50x eyepiece (NA 0.75). A single airy diffraction pattern suggests a point source, which cannot be resolved by a microscope [31].
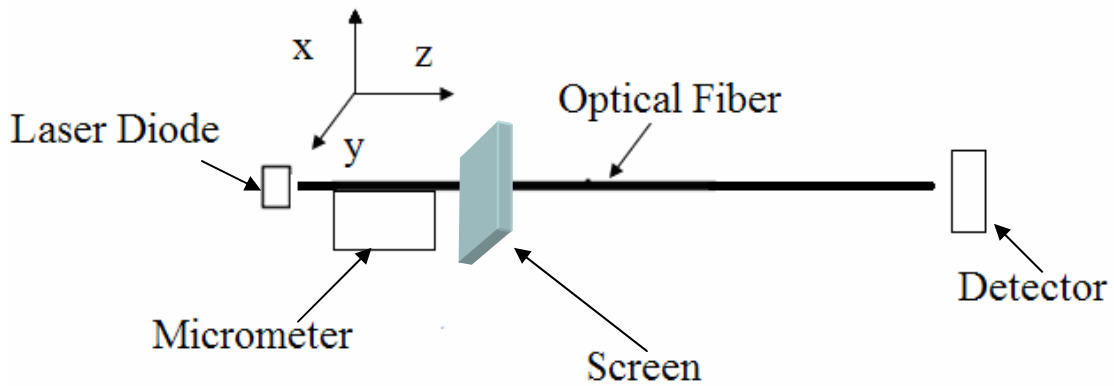
Figure 3.1 Schematic of the light coupling setup

The light from the fiber is collected with a UDT-PIN-10D detector which has a diameter of about 1 cm. A battery is connected in series to the photodiode and I apply a reverse bias voltage of 9V, so as to operate it in photoconductive mode. This helps to improve the speed of response. The AC voltage drop across a 100kΩ resistor is measured using a lock-in amplifier. The output power through a polarizer is measured, while keeping the input laser current at 35.2±0.2mA. As we rotate the polarizer by 360° the intensity of the light through polarizer follows Malus's law, i.e.

$$I = I_0 \cos^2 \theta \qquad\qquad (2) ,$$

which indicates that it is indeed a plane polarized light. Here I_0 is the intensity when

polarization axis of the polarizer is along polarization coming out of the fiber. θ is the

angle between incident polarization and the polarization axis of the polarizer. Fig 3.2

shows the optical intensity as a function of polarizer angle for an aperture shown in

Fig 2.8. The tips have a typical ratio of maximum and minimum signal intensities of

about 100 to 1, so that we may define the

Extinction ratio ER = 10 log (Pmax / Pmin)   (3)

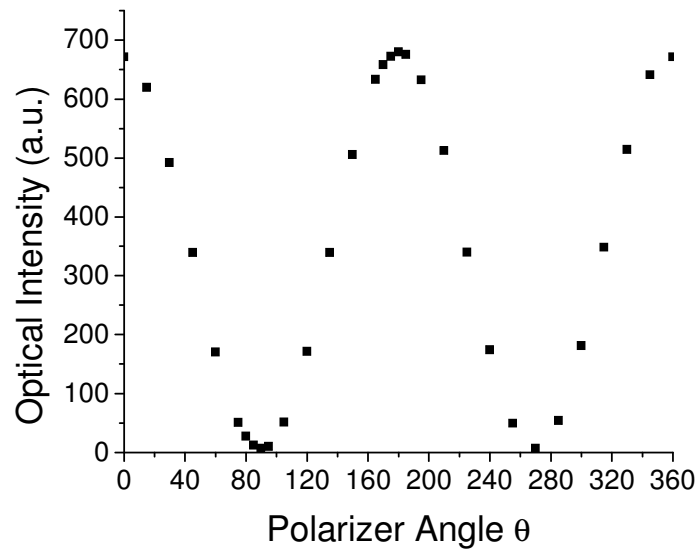$\approx$ 10 log100 = 20, as a measure of degree of polarization.

Fig 3.2. Light intensity as a function of polarizer angle.

To determine whether the fiber probe maintains the polarization, incident polarization

is rotated by 90º, and the experiment is repeated. I found that the output also has a

phase shift of 90º.

3.3 Throughput of the Probes

The throughput of the fiber probe is defined as the ratio of output to the amount of incident light onto the fiber. Next I would like to discuss the mechanisms leading to lower throughput in a NSOM probe. For incident light polarized along the x direction, onto to a perfectly conducting screen in the xy plane, with a circular aperture smaller than the wavelength of the light, the Bethe [36] solution to electromagnetic fields in the far field gives:

$$E_x = 2E_0 k^2 a^3 z e^{ikr}/3\pi r^2 (1-1/ikr), \tag{4}$$

$$E_z = 2E_0 k^2 a^3 x e^{ikr}/3\pi r^2 (1-1/ikr) \text{ when } |r| \gg a, \tag{5}$$

where a is the aperture diameter and k is the propagation constant. The far field light intensity from this radiating magnetic dipole falls off as a^6/λ^4.

Boukamp [37, 38] showed that the Bethe's solution in the near field doesn't satisfy the boundary conditions. His correction shows a light intensity, which is higher than predicted by Bethe in the near-field.

$$E_x \propto ikz - \frac{2}{\pi} ikau \left[1 + v\tan^{-1} v + \frac{1}{3(u^2+v^2)} + \frac{x^2-y^2}{3a^2(u^2+v^2)(1+v^2)^2} \right], \tag{6}$$

$$E_y \propto -\frac{4ikxyu}{3\pi a(u^2+v^2)(1+v^2)^2}, \qquad E_z \propto \frac{4ikxv}{3\pi(u^2+v^2)(1+v^2)}. \tag{7}$$

Where

21

$$z = auv, \quad x = a\sqrt{\left(1-u^2\right)\left(1+v^2\right)}\cos\varphi, \quad y = a\sqrt{\left(1-u^2\right)\left(1+v^2\right)}\sin\varphi.$$

The out-coming fields are strongly dominated by E_x followed by E_z and E_y components. Even though our apertures are in elliptical shape, the Bethe's solution gives an idea about the loss of the light intensity when we push it through a sub wavelength aperture. The throughput of the fiber also depends on the ability of a metal coated waveguide to support the TE_{11} mode beyond its cut-off. As the mode goes from a propagating wave to an evanescent wave the light intensity drops exponentially. The tapered etched tips have a higher cone angle compared to the pulled tip, which results in evanescent wave traveling less distance leading to a higher throughput. In mechanically pulled tips the core is tapered over a longer distance compared to the etched tips and the light leaks out from the core, which causes more loss. Etched tips have their cores tapered at the very end as in figure 3.3. One more advantage with chemical etching is that we can control the shape of the final aperture formed so as to enhance the optical transmission. The elliptical shape of our sub wavelength aperture results in a polarization dependent throughput [39] because of the boundary conditions imposed, i.e. $E_\parallel = 0$ at the surface of a conductor. This condition squeezes the output when the polarization is along the major axis. The light output is maximum when polarization is along minor axis. This is because of the higher surface currents induced around the aperture by the electric field which results in stronger induced magnetic and electric dipoles. In this case the distance between the induced magnetic dipoles is higher compared to the distance between induced

dipoles when polarization is along major axis. As the distance between the dipoles becomes smaller their fields tend to cancel each other.
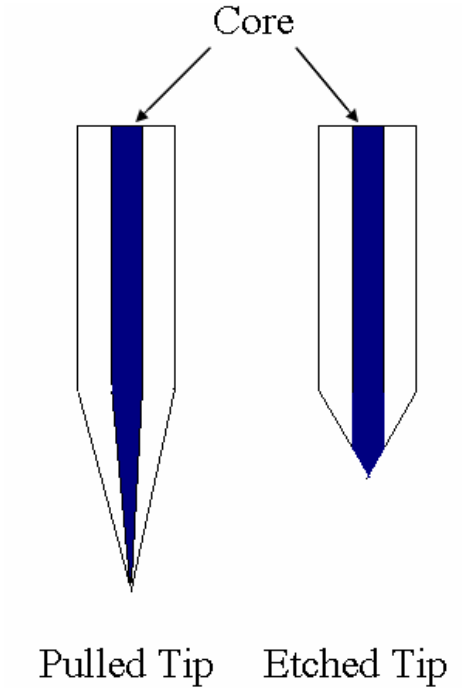
Figure 3.3 Comparison of etched tip and a pulled tip. Pulled tips have typical taper lengths of 2 mm. Etched tips have taper lengths of about 150-300 µm depending on the diameter of the fiber.

The throughput of the fibers is measured by comparing the light coming out of the fiber to that of the fiber with a tip. Since the laser diode used to launch the light has a beam divergence, some of the light goes into the cladding. To compare the power coming out of the two fibers, we have to make sure that the cladding modes are well attenuated by polymer jacket which has a higher refractive index than the cladding. To determine the minimum length of the jacket to appreciably remove the cladding

modes, I measured the light coming out of the fiber with different jacket lengths.
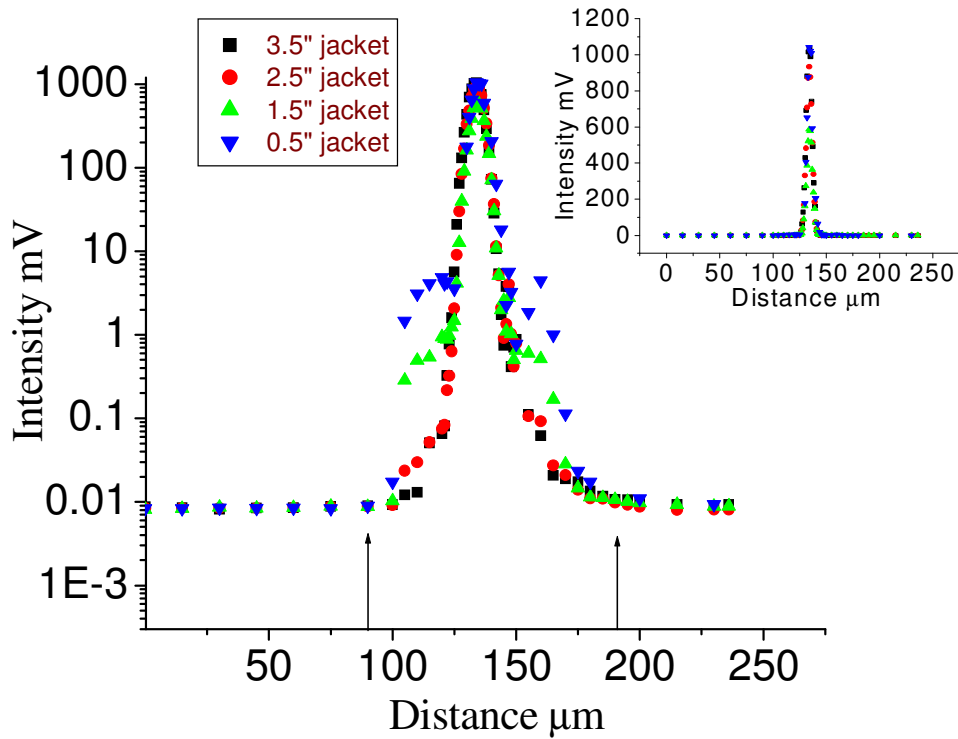
Figure 3.4. Logarithmic plot of voltage measured across a 100K resistor vs. the lateral distance traveled with respect to a polarized laser beam. The peak voltage corresponds to a power of about 20 μW. Arrows indicate beginning and end of the fiber. Inset shows the same values on a linear scale. FWHM ≈ 5 μm

Experiments are done using the same conditions mentioned above except that distance between laser and fiber was kept at approximately 50 µm and light is directly collected by detector. The fiber produced a shadow of 1.5" diameter on a screen placed at a distance of 1.75" from the laser. The fiber is moved across the laser diode, with major axis parallel to the electric field. The voltage drop across a resistor is measured using an AC voltmeter after amplification. This experiment is repeated

with different reduced jacket lengths. I found that a minimum of 3″ jacket is necessary to attenuate the cladding modes atleast by a factor of 10^5 as shown in figure 3.4. The arrows indicate the beginning and the end of the fiber. The intensity of the light is maximized for each measurement, by adjusting the micrometer, while keeping the distance between the diode and the fiber as constant.

I measured the output of several different cleaved fibers in the same setup but increased the distance between the laser diode and fiber to 150 µm. The laser diode has a Gaussian intensity profile. As fiber is moved away from the diode, small changes in the lateral position of the fiber don't lead to significant change in the incident power. The fiber is mounted with its minor axis parallel to the electric field. Power coming out of the fibers varied with less than 15% deviation from fiber to fiber. This shows the margin of error for the throughput measurement.

Any incident plane polarization onto the bare elliptical core fiber is split into two perpendicular components along major and minor axis respectively. These components travel at different velocities [27]. The polarization is preserved if the incident electric field is incident along the major or minor axis. For any other polarization directions output light will have an elliptical polarization or a plane polarization depending on the length of the fiber. For an aluminum coated fiber probe with very small elliptical apertures, component of the field along major axis undergoes a much higher attenuation compared component along the minor axis and hence

$$I_{out} \approx I_0{}^2\cos^2\theta \qquad\qquad (8)$$

25

where θ is the angle between incident electric field and the minor axis of the fiber. I_0 is the intensity coming out of the probe when the incident field is along the minor axis. Hence the fiber probe acts like a polarizer with polarization axis along the minor axis.

Fibers are placed at approximately 150 microns from the laser diode, which produced a shadow of diameter 0.75″ on a screen placed at a distance of 1.75″ from the laser diode. Probes are placed approximately 1 mm from the detector to collect maximum light from the point source with the incident electric field parallel to the minor axis in the beginning. The voltage drop across a 100kΩ resistor is measured using a lock-in amplifier. Figure 3.5 shows the typical optical intensity from the probes as a function of direction of incident polarization. Each of the data points is taken by maximizing the output by adjusting the lateral position of the fiber using micrometer while keeping the distance between the fiber and the laser diode at approximately 150 microns. A bare fiber having a jacket length of 7 inches placed at same distance from the laser diode has an out put of 781.2mV for polarization along minor and major axis respectively. The intensity vs incident polarization data for a tip with minor axis aperture sizes ranging from 20 ± 5 nm to 150 ± 5 nm are taken. Maxima and minima are used for throughput calculations. All the fibers had a jacket length of at least 7 inches. Figure 3.6 shows the throughput of the tips as a function of the minor axis dimension for both polarizations and also for pulled tips [40]. We have been successful in obtaining a throughput of 10^{-3} for an aperture dimension of 20±5 nm by 100±5 nm.
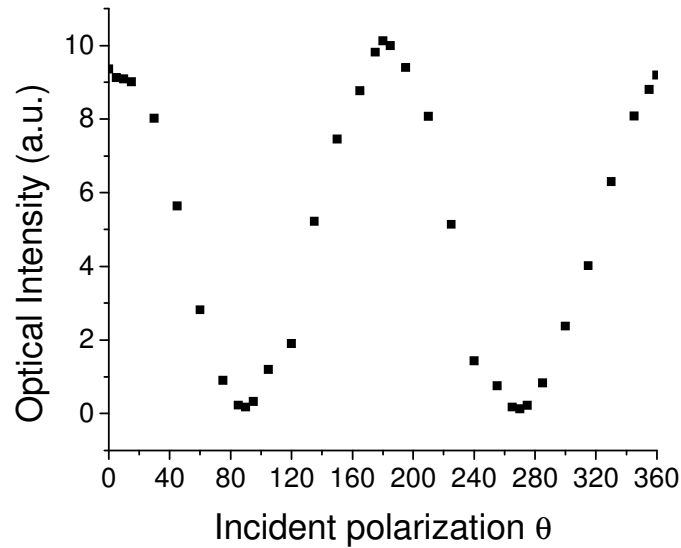
Figure 3.5. Typical light intensity as a function of incident polarization. This measurement was done using a probe having an aperture dimension of 55 ± 5 nm by 220 ± 5 nm.

The throughputs of these tips are orders of magnitude higher than the reported throughputs of the tips obtained with pulling and chemical etching techniques. This is because of the elliptical shape of our aperture and also higher cone angle of our tapered probe. The aspect ratios of the apertures are not always a constant as seen in figure 3.7. This is because of the variations in etching conditions and the position of the FIB cut.
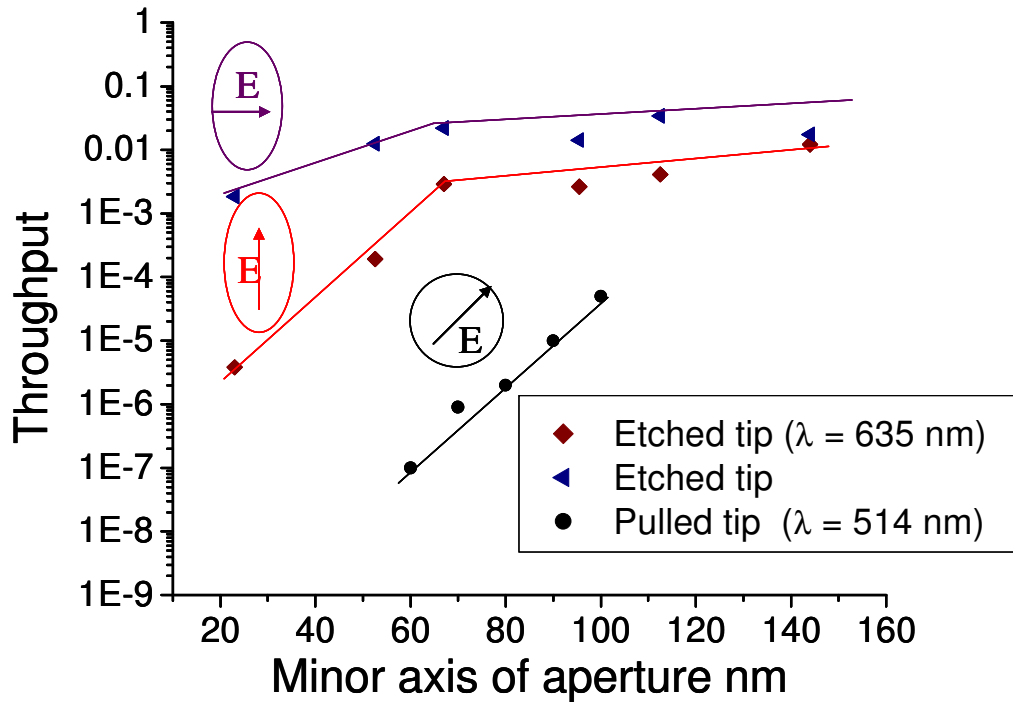
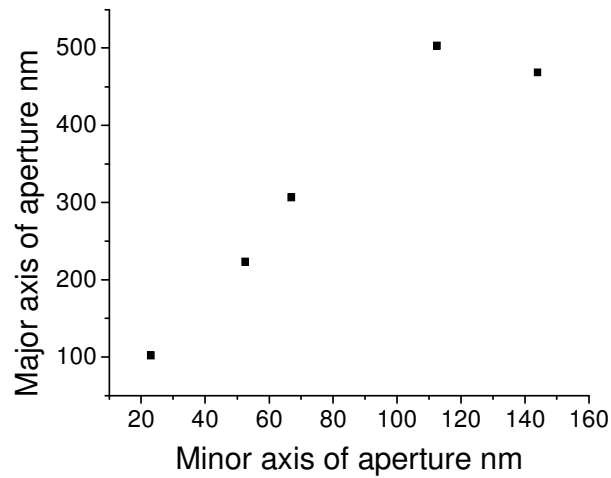Figure 3.6 Throughput of the tips as a function of minor axis dimension.

Figure 3.7 Major axis dimensions of the tips used for throughput measurement.

4. Near-Field Scanning Optical Microscopy

4.1 Tip-sample feedback

Keeping the distance between the tip and sample constant during NSOM imaging is important to avoid artificial contrast during the scanning. To accomplish this, the tip is vibrated parallel to the sample, and as the probe-sample distance gets smaller than 30 nm [12] the amplitude of vibration decreases due to the interaction between the tip and the sample which will be detected by a feedback circuit. The nature of interaction between them is not clear [41, 42, and 43]. In the feed-back circuit we can specify amplitude and it will maintain it by sending a voltage to the piezoelectric stage which will move closer or farther to the tip depending on the amplitude of vibration. To measure the amplitude of the vibration of the tip it is glued onto a quartz tuning fork [44, 45, and 46]. While doing the scans the tuning fork is vibrated at its resonance (about 33.2 KHz) by a piezoelectric quadrant tube with amplitude of about 20 μV rms or approximately 0.75nm-rms [44]. An induced strain in the piezoelectric quartz tuning fork produces a voltage, which is measured using a lock-in amplifier. The detail of the entire set-up is described elsewhere [31]. A proportional-Integral (PI) circuit was used to hold the amplitude of vibration about 3% lower than the free amplitude. A typical approach curve for an NSOM tip is given in Fig 4.1 [15]. Figure 4.2 shows a block diagram of crucial elements of the feedback circuit. When the set point is equal to the tuning fork amplitude, the output of proportional will be zero but the integral will hold the output to a dc value. The time response of the changes in circuit is also controlled by the integral which includes a convolution of tuning fork response, lock-in response and PI response, which is about 20ms.
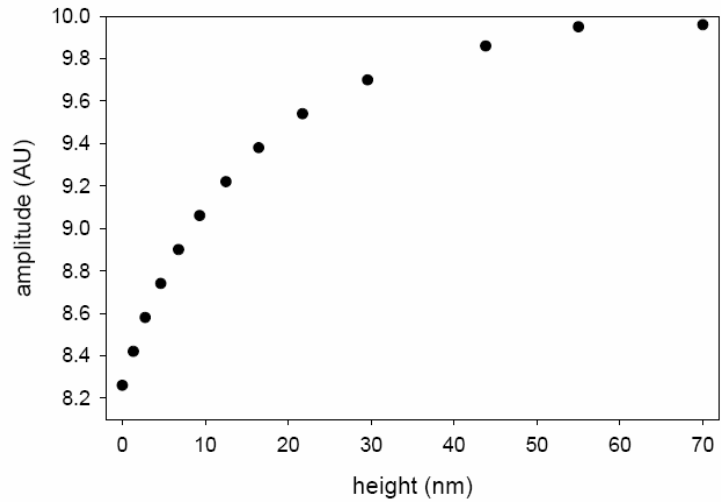
Figure 4.1 Approach curve for NSOM probes. Vibration amplitude with the height of
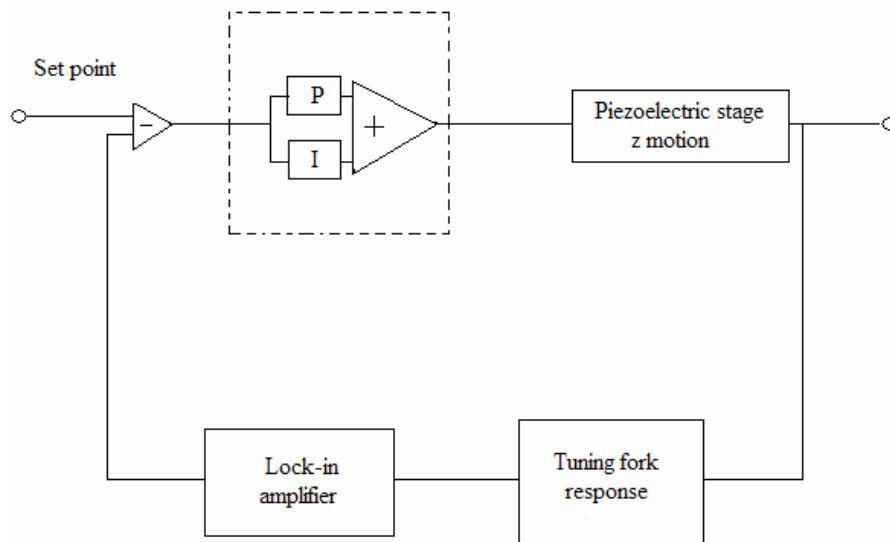
the tip above the sample.

Fig 4.2 Block diagram of feedback mechanism to control Tip-sample separation

4.2 Near Field Scanning Optical Microscope Operation and Light Collection

The images collected for this thesis were obtained by operating an NSOM in reflection mode [47] , i.e. the tip was used as an illuminator and the reflected light from the sample was collected using a microscope objective with NA=0.4 and at 30° to the sample as shown in Fig 4.3.
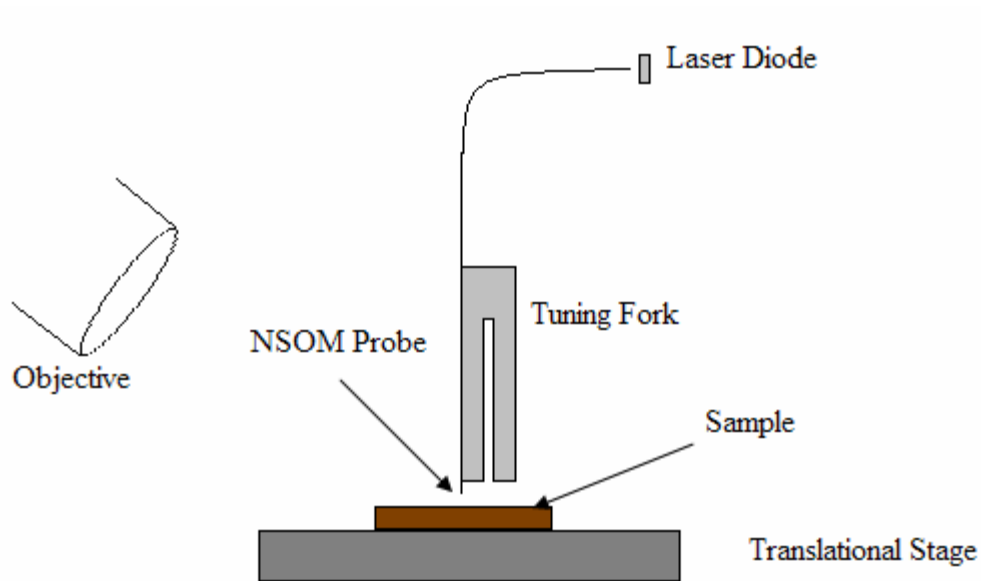
Figure 4.3 Schematic of NSOM setup.

Modulated light from the laser diode (λ=635nm) is launched onto the cleaved fiber, with polarization along the minor axis so as to get higher throughput. The fiber probe is oriented by placing a polarizer between the detector and the probe and it is rotated until the maximum intensity is reached. At this position the minor axis of the probe is parallel to the polarization axis of the polarizer. The probe is locked in that position and is glued onto the tuning fork. The plane involving detector and probe was placed

perpendicular to the minor axis of the aperture to collect the maximum light. Light with such a polarization will induce dipoles in the same direction in the sample, which will be able to radiate the light mostly in the plane containing the detector and the fiber probe. This was indeed proved by experimental evidence [14]. Orienting the fiber also helps to reveal the direction of scan in which the resolution will be a maximum. To characterize the tips they are scanned on Au dots on a GaAs substrate. The dots have a range of diameters from about 0.7 µm to 8 µm and a height of about 30 nm. Light collected in reflection mode is about 100 times lower intensity than the throughput of the probe. The reasons for this can be attributed to the shadowing effect by the aluminum coating surrounding the aperture and the plateau surrounding the central tip and also the position of the detector.
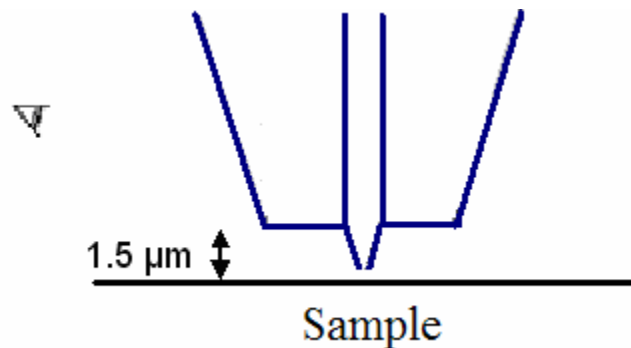
4.4 Schematic of the shadowing effect. As the tip gets closer more light will be blocked by the plateau and the aluminum coating surrounding the aperture

Fig 4.5a shows a plot of the light intensity vs. distance between the probe and the sample. When the probe is far way from the sample, the intensity of the collected light is low. As the tip moves closer to the sample the intensity increases by 30 fold since the image of the probe comes to the focus of the microscope. As we move the

tip very close to the sample the intensity falls off rapidly due to the shadowing of the light by the coating surrounding the probe and the reflected light also gets blocked by plateau. When the distance between the tip and the sample d is of the order of 50 microns or less, the intensity reaching the detector oscillates as the sample moves close to the detector as in Figure 4.6. This can be attributed to the interference between incident light from the tip and reflected light from the sample and from the plateau, which forms a standing wave [48, 49, 50, 51]. Figure 4.5b shows the trough to peak ratio of the collected light intensity oscillations with distance between tip and sample. Figure 4.5a is created by taking the median of these oscillations. Oscillations have a period of $\lambda/2$.

When the tip is very close to the sample, light can undergo multiple reflections because of the presence of the plateau which results in oscillations with varying period as in figure 4.6 b.
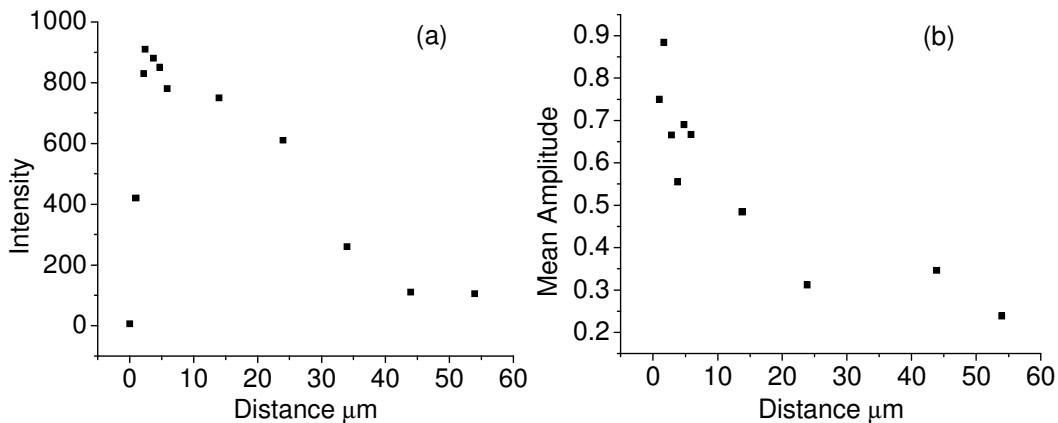
Figure 4.5 (a) Light intensity as a function of tip-sample separation. (b) Trough to peak ratio of the oscillations as a function of tip-sample separation.
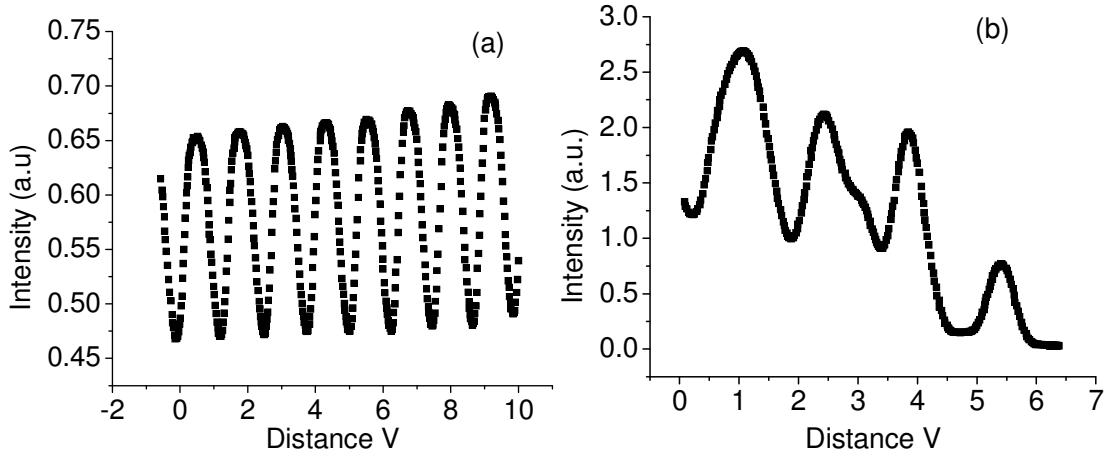
Figure 4.6 Interference effect in close proximity to the sample: Intensity as a function of distance between tip and the sample when the initial gap between tip and sample is approximately (a) 1.1 μm and (b) 44 μm respectively. Period of oscillations is approximately 330nm. 1 volt corresponds to 0.266 μm. Intensity plots are obtained with a tip having an aperture of 50nm by 200nm.

4.3. Light Intensity and Topographical images

Factors that affect reflection NSOM imaging include shadowing, the angle of light collection and collection geometry. Apart from shadowing effects due to the coating of the tips as described above, there are shadowing effects due to the topography of the sample. As the angle to the sample normal increases more light is collected [52]. Scanning was done using a program written with Lab-view software. Raster scanning was done with a step size of 20 nm while keeping the minor axis parallel to the line scan. The program allowed the probe to oscillate for desired time about each image spot before moving onto the next spot. For the scanning I used a wait time of 50 ms. Figure 4.7 shows the NSOM scans on gold dots scanned with a tip having an aperture of 20 nm by 100 nm coated with about 300 nm of aluminum.

34

The microscope objective was placed in the upper side of the image. The left side of the images (a) and (b) show the Intensity and topographical scans obtained by moving the stage left to right. To take into account the piezo hysteresis and the sample tilt a background is subtracted from topographic images. The size of the tip increases the apparent dot size in the topographic image. Many of the effects, including the bright and dark edges can be explained using simple effects of topography playing a role in contrast. Some of the artificial contrast mechanisms because of the topography and location of the detector are shown in Figure 4.8 [53, 54, 14]. The dots appear to have lower reflectance compared with the GaAs matrix. This is contrary to the results observed by Kolb [15]. I will discuss this by considering aluminum coated tip in close proximity to sample (d<< λ) as a waveguide. The output of this waveguide is sensitive to the nature of the sample i.e. it depends on how well the waveguide can support E_x or E_z. The boundary conditions require a continuity of the tangential fields. Modes from E_x are cut-off since the distance between tip and the sample is much smaller than λ. When the tip is on a metal E_x is more severely affected by the boundary conditions compared to when it is on GaAs. E_z is not so much restricted by boundary conditions. This was demonstrated experimentally by Durkan and Shvets [55] where they compared the polarization state of the light in the near field to same when the tip is pulled back. According to their results, they have not observed any changes in polarization state from near-field to far field for insulators but they did for metals. We can expect the amount of light to the detector to depend on the thickness of the Al coating. Since E_x constitutes a major portion of the field coming out of the probes, the thicker the coating the lower will be the amount of light collected.
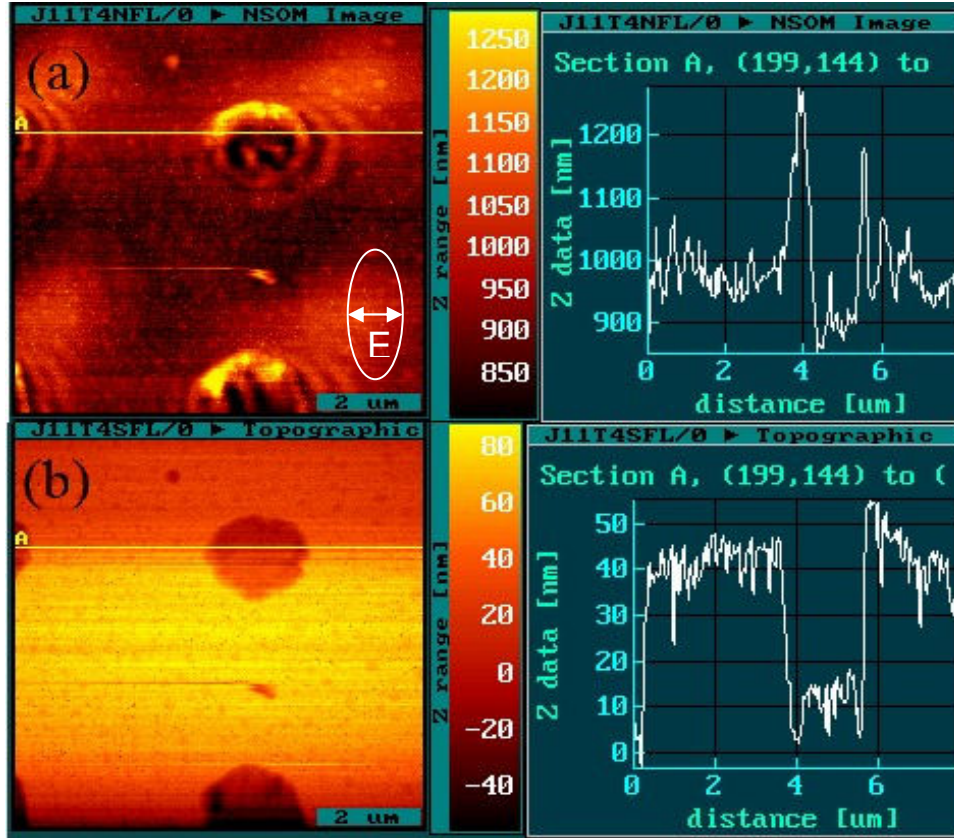
Figure 4.7   NSOM scans of 1.4 µm diameter gold dots on GaAs substrate. a)

Intensity scan b) Topographical scan showing a dot height of about 35 nm. Line scans

are also shown. Topographic scans are inverted.

Probes used for this NSOM scan have a coating of 300nm, which is much higher than

usually used tips. Since E_x gets severely restricted by the boundary conditions and

very thick coating, Ez could constitute a major portion of the light coming out of

these probes. On GaAs however the E_x component is not as much restricted and we

can expect a jump in the reflectance.
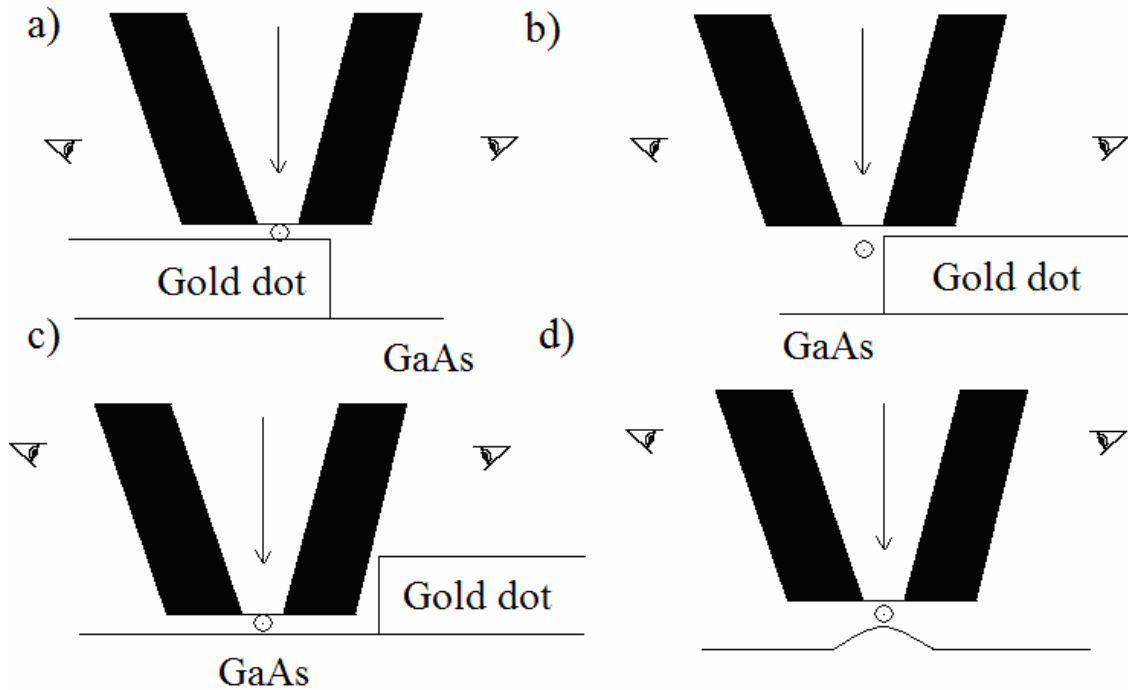
Figure 4.8   Artificial contrasts due to topography.   (a) More (normal) (b) Less (more) (c) Less (normal) (d) More (more) light is collected by right (left) detector. Direction of the incident electric field (represented by small circle) is perpendicular to the plane involving the detector and the probe.

We can see interference rings surrounding the dots. These are due to the interference between the reflected light from the dot and the light from the tip.   Interference effects due to topography have been reported earlier in many other cases [56] and some of the mechanisms responsible for these effects were discussed [57].   A preferential direction of the rings (i.e. to the right and left side of the dots) is due to the position of the detector. Light gets shadowed by either tip or the dot in other directions. As the tip moves farther from the dot only a small portion of the light will reach the dot, hence amplitude of interference rings decreases. Interference effect can be explained with a simple model. As the light reflects from the gold it under goes a

phase shift which has to be included in path difference calculations. In Figure 4.9 the path difference between two light rays, for constructive interference is

$$L - h = (m+1/2)\lambda, \text{ m is an interger} \tag{9}$$

$$L^2 = [(m+1/2)\lambda + h]^2 \tag{10}$$

$$[R\sin\theta]^2 + [d-R\cos\theta]^2 = [(m+1/2)\lambda + R\sin\theta]^2 \tag{11}$$

$$d = \{[(m+1/2)\lambda]^2 + 2R(m+1/2)\lambda\sin\theta\}^{1/2} + R\cos\theta \tag{12}$$

with conditions that,

Maximum θ for any d is, when ray is a tangent to the dot.

$$\theta_{max} = \cos^{-1}(R/d), \tag{13}$$

The other condition is that the reflected light from the dot has to be at 90° with respect to the line joining probe and the center of the dot to reach the detector.

Which gives $\tan 2\theta = [d-R\cos\theta] / R\sin\theta$

$$=> \cos2\theta = R\cos\theta / d = \cos\theta_{max} \times \cos\theta \tag{14}$$

These two conditions give d values of 1.1746 μm and 1.8887 μm for m = 0 and 1 respectively, which correspond a θ value of 29.22 ° and 36.09 °. Experimentally observed values for d are

1.333 μm (Left Scan), 1.222 μm (Right Scan)   for m = 0

and   1.8518 μm (Left Scan), 1.593 μm (Right Scan)   for m = 1

(a)

Detector

(b)
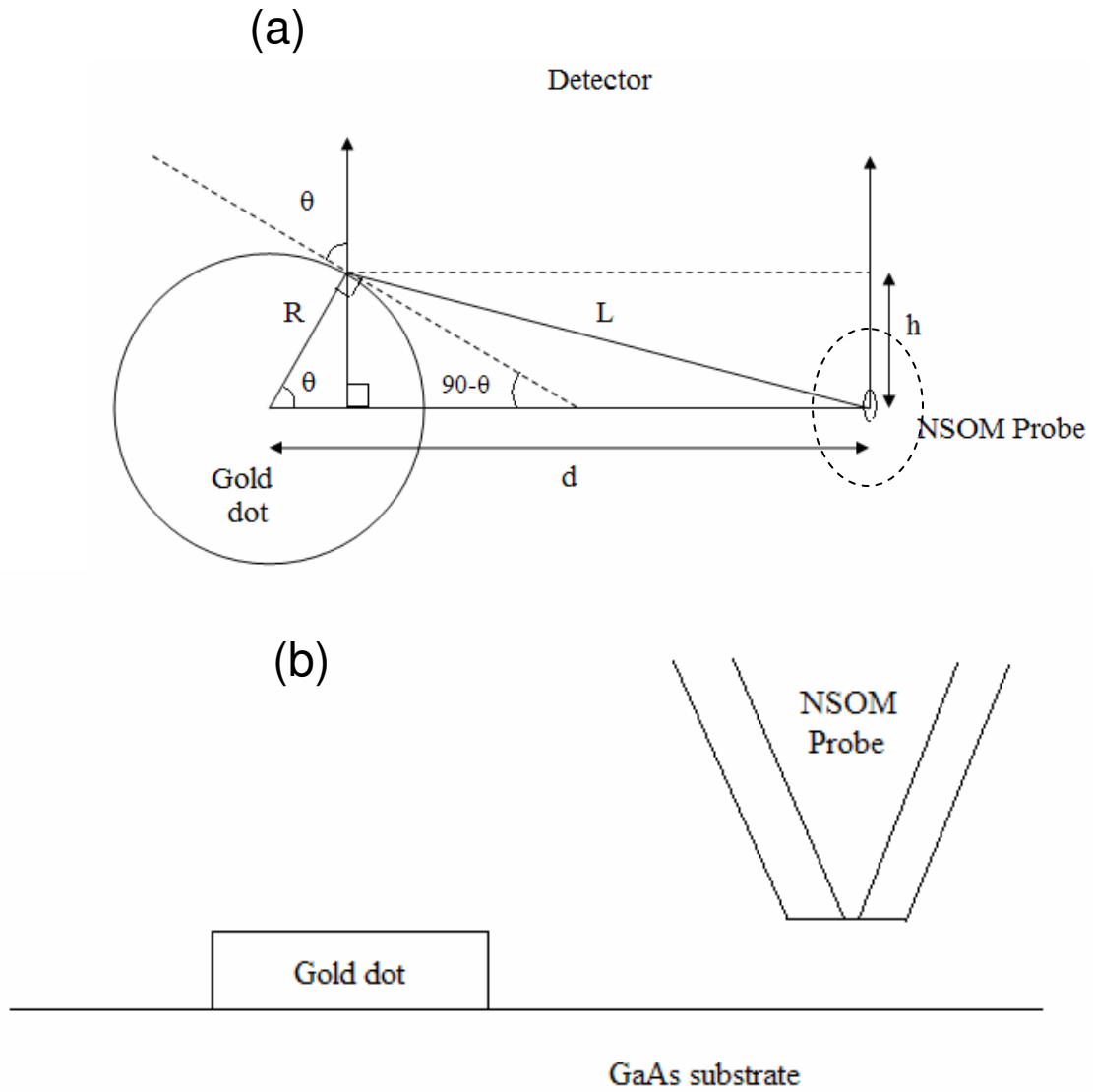
Figure 4.9 Schematic representation of interference effect. (a) Top view (b) Side view

There are several factors which are not taken into account in this calculation. They

are:

    1) The distances involved in this calculation are of the order of λ, hence we

        have to take into account the boundary conditions for electromagnetic

        fields.

2) The dots may not be perfectly circular, and I have not taken into account the effects of the circular nature of the reflecting surface.

3) There could be a phase difference between the light propagating in perpendicular directions because of the ellipticity the probe.

However, the model gives a general idea of interference affects due to the topography and is in reasonable agreement with the experiment.

5. Summary

The thesis has successfully demonstrated a chemical etching technique to reproducibly fabricate polarization maintaining NSOM probes. The probes obtained by the process have a polarization dependent throughput. The throughput of the tips is much higher than the conventional etched and pulled tips for the same aperture dimensions. The tips will immensely improve the ability of NSOM to conduct experiments which require high throughput and resolution such as Raman Scattering, Single molecule fluorescence and Photoluminescence of quantum dots. The polarization maintaining capability of probes will enhance the ability to understand the data gathered from these experiments.

The Near-field images of gold dots presented here have shown that the probes can be operational as NSOM in reflection mode. The images do not easily allow the determination of the spatial resolution of tips because the optical response was dominated by topographic effects. We have shown that the probes can engage the sample very well and the images show the basic behavior which were observed in the earlier experiments. The tips are expected to show a very good resolution in one dimension, and a demonstration of this on a topography free sample which has a strong polarization dependent optical contrast is anticipated to provide an insight into the scope of these probes as a powerful characterization tool. Future work to be done includes improving the morphology of the probes by reducing the amount of aluminum on the probes, reducing the diameter of the plateau surrounding the tip and demonstrating the resolution of the probes by conducting single molecule fluorescence experiment on chromophores.

Bibliography

[1] E. H. Synge, "A suggested model for extending microscopic resolution into the ultra-microscopic region," *Philosophical Magazine* **6,** 356 (1928).

[2] E. A. Ash and G. Nicholls, "Super-Resolution Aperture Scanning Microscope," *Nature* **237,** 510 (1972).

[3] D .W. Pohl, W. Denk and M. Lanz, "Optical Stethoscopy: Image recording with resolution λ/20," *Applied Physics Letters* **44**, 651-653, (1984).

[4] E. Betzig, J.K. Trautman, T.D. Harris, J.S. Weiner, and R.L.Kostelak, "Breaking the Diffraction Barrier: Optical Microscopy on a Nanometric Scale" *Science* **251**, 1468-1470, (1991).

[5] K.M. Takahashi, "Meniscus Shapes on Small Diameter Probes," *Journal of Colloid and Interface Science* **134**, 181-187, (1990).

[6] P. Hoffmann, B. Dutoit, and R.P. Salathe, "Comparison of mechanically drawn and protection layer chemically etched optical fiber tips," *Ultramicroscopy* **61**, 165, (1995).

[7] T. Pangaribuan, K. Yamada, S. Jiang, H. Ohsawa, , M. Ohtsu, "Reproducible Fabrication Technique of Nanometric Tip Diameter Fiber Probe for Photon Scanning Tunneling Microscope", *Japanese Journal of Applied Physics* **31**, L1302, (1992).

[8] V. Deckert, D. Ziesel, R. Zenobi, and T. Vo-Dinh, "Near-field surface-enhanced Raman imaging of dye-labeled DNA with 100nm resolution," *Analytical Chemistry* **70,** 2646–2650, (1998).

[9] D. Ziesel, V. Deckert, R. Zenobi, and T. Vo-Dinh, "Near-field surface-enhanced Raman spectroscopy of dye molecules adsorbed on silver island films," *Chemical Physics Letters* **283,** 381–385, (1998).

[10] N. Hosaka and T. Saiki*, "Near-field fluorescence imaging of single molecules with a resolution in the range of 10 nm," *Journal of Microscopy* **202**, 362-364, (2001).

[11] K. Matsuda, T. Saiki, S. Nomura, M. Mihara, Y. Aoyagi, S. Nair, and T. Takagahara, "Near-field optical mapping of exciton wave functions in a GaAs quantum dot," *Physical Review Letters* **91,** (2003).

[12] E. Betzig, P.L.Finn and J.S.Weiner, "Combined shear force and near-field scanning optical microscopy," *Applied Physics Letters* **60**, 2484-2486, (1992).

[13] E. B. McDaniel and J. W. P. Hsu, "Nanometer scale optical studies of twin domains and defects in lanthanum aluminate crystals," *Journal of Applied Physics* **80,** 1085, (1996).

[14] J. A. Cline and M. Isaacson, "Probe-sample interactions in reflection near-field scanning optical microscopy," *Applied Optics* **34,** 4869 (1995).

[15] P. W. Kolb, *Cryogenic near-field scanning optical microscopy: quantum dots, charge-ordered domains, and ferromagnetic nucleation,* Ph.D. Thesis, University of Maryland, (2004).

[16] E. Betzig, J. K. Trautman, J. S. Weiner, T. D. Harris, and R. Wolfe, "Polarization contrast in near-field scanning optical microscopy," *Applied Optics* **31,** 4563 (1992).

[17] G. A. Valaskovic, M. Holton, and G. H. Morrison, "Image-contrast of dielectric specimens in transmission mode near-field scanning optical microscopy - imaging properties and tip artifacts," *Journal of Microscopy-Oxford,* **179,** 29 (1995).

[18] E. Betzig and R. J. Chichester, "Single Molecules Observed by Near-Field Scanning Optical Microscopy," *Science* **262**, 1422, (1993).

[19] E. Betzig, J. K. Trautman, R. Wolfe, E. M. Gyorgy, and P. L. Finn, "Near-field magneto-optics and high density data storage," *Applied Physics Letters* **61**,142, (1992).

[20] Katsunari Okamoto, *Fundamentals of Optical Waveguides*, (Academic Press, 1992) pp 107.

[21] C. Yeh, "Elliptically Dielectric Waveguides," *Journal of Applied Physics* **33**, 3235, (1962).

[22] V. Ramaswamy, W. G. French, and R. D. Standley, "Polarization Characteristics of Noncircular Core Single-Mode Fibers," *Applied Optics* **17**, 3014, (1978).

[23] R. H. Stolen, V. Ramaswamy, P. Kaiser, and W. Pleibel, "Linear Polarization in Birefringent Single-Mode Fibers," *Applied Physics Letters* **33**, 699, (1978).

[24] V. Ramaswamy, I. P. Kaminow, P. Kaiser, and W. G. French, "Single Polarization Optical Fibers: Exposed Cladding Technique," *Applied Physics Letters* **33**, 814, (1978).

[25] I. P. Kaminow, J. R. Simpson, and H. M. Presby, "Stain Birefringence in Single-Polarization Germanosilicate Optical Fibers," *Electronics Letters* **15**, 677 (1979).

[26] Mitsui, T. and Sekiguchi, T., "Observation of polarization property in near-field optical imaging by a polarization-maintaining fiber probe," *Journal of Electron Microscopy* **53(2)**, 209-215, (2004).

[27] R.B. Dyott, *Elliptical Fiber Wave guides*, (Artech House Publishers, 1995)

[28] R. K. Varshney and A. Kumar, "Effect of Depressed Inner Cladding on the Polarization Characteristics of Elliptical Core Fiber," *Optics Letters*.**9**, 522 (1984).

[29] M. Ohtsu, *Near-Field Nano/Atom Optics and Technology*, (Springer-Verlag, Tokyo, 1998).

[30] Raoul Stockle, Christian Fokas, Volker Deckert, and Renato Zenobi, Beate Sick, Bert Hecht, and Urs P. Wild, "High Quality Near-Field Probes by Tube Etching", *Applied Physics Letters* **75**, 160, (1999).

[31] B.S. Palmer, *Development and Applications of Scanning Probe Techniques: Scanning Eddy Current Dynamometer and Photoconductivity Studies of Underdoped YBCO*, Ph.D. Thesis, University of Maryland, (2003).

[32] Masaru Muranishi, Kazutaka Sato, Sumio Hosaka, Atsushi Kikukawa, Toshimichi Shintani and Kenchi Ito, "Control of Aperture Size of Optical

Probes for Scanning Near-Field Optical Microscopy Using Focused Ion Beam Technology," *Japanese Journal of Applied Physics* **36**, L942-L944, (1997).

[33] Th. Lacoste, Th. Huser, R. Prioli, H. Heinzelmann, "Contrast Enhancement using Polarization-modulation Scanning Near-field Optical Microscopy (PM-SNOM)," *Ultramicroscopy* **71**, 333-340, (1998).

[34] J. A. Veerman, M. F. Garcia-parajo, L. Kuipers and N. F. Van hulst, "Single molecule mapping of the optical field distribution of probes for near-field microscopy," *Journal of Microscopy* **194**, 477-482, (1999).

[35] J. A. Veerman, A. M. Otter, L. Kuipers and N. F. van Hulst, " High definition aperture probes for near-field optical microscopy fabricated by   focused ion beam milling" *Applied Physics Letters* **72**, 3115, (1998).

[36] H.A. Bethe "The Theory of Diffraction by Small Holes" *The Physical Review*, **66**, 163-182, (1944).

[37] C.J. Bowkamp, "On Bethe's Theory of Diffraction by Small Circular Disks and Holes" *Philips Research Reports* **5,** 321-332, (1950).

[38] C.J. Bowkamp, "On the Diffraction of Electromagnetic waves by Small Circular Disks and Holes" *Philips Research Reports* **5**, 401-422, (1950).

[39] A.R. Zakharian, M. Mansuripur and J.V. Moloney, "Transmission of light through small elliptical apertures," *Optics Express* **12**, 2631, (2004).

[40] G.A.Valaskovic, "Parameter control, characterization, and optimization in the fabrication of optical fiber near-field probes", *Applied Optics* **34**, 1215, (1995).

[41] C. Durkan, I.V. Shvets, "Investigation of physical mechanisms of shear-force imaging" *Journal of Applied Physics* **80**, 5659, (1996)

[42] S. Davy, M. Spajer, and D. Courjon, "Influence of the water layer on the shear force damping in near-field microscopy", *Applied Physics letters* **73**, 2594, (1998).

[43] M. K. Gregor, P. G. Blome, J. Scho¨fer, and R. G. Ulbrich, "Probe-surface interaction in near-field optical microscopy: The nonlinear bending force mechanism," *Applied Physics Letters* **68**, 307, (1996).

[44] K. Karrai and R.D. Grober, "Piezoelectric tip-sample distance control for near field optical microscopes" *Applied Physics Letters* **66**, 1842-1844 (1995).

[45] K. Karrai and R.D.Grober, "Piezoelectric tuning fork tip-sample distance control for near field optical microscopes" *Near Field Optics and Related Techniques* (Digest series: vol.8) **61**, 197-205, (1995).

[46] R. D. Grober, J. Acimovic, J. Schuck, D. Hessman, P.J. Kindlemann, J. Hespanha, A. S. Morse, K. Karrai, I. Tiemann and S. Manus, " Fundamental limits to force detection using quartz tuning forks" *Review of Scientific Instruments* **71**, 2776-2780, (2000).

[47] M.A. Paesler and P.J. Moyer, *Near-Field Optics: Theory, Instrumentation, and Applications*, (Wiley-Interscience, New York, 1996).

[48] P. G. Gucciardi, M. Labardi, S. Gennai, F. Lazzeri, M. Allegrini, "Versatile scanning near-field optical microscope for material science Applications" *Review of Scientific Instruments* **68**, 3089, (1997)

[49] B. Hecht, H. Bielefeldt, D. W. Pohl, L. Novotny, H. Heinzelmann, "Influence of detection conditions on near- field optical imaging," *Journal of Applied Physics* **84**, 5873, (1998).

[50] U. Ch. Fisher, U.T. Duriq, D.W. Pohl, "Near-field Optical Scanning Microscopy in Reflection," *Applied Physics Letters* **52**, 249, (1988).

[51] M. Labardi, P.G. Gucciardi, M. Allegrini, C. Pelosi, "Assessment of NSOM resolution on III-V semiconductor thin films," *Applied Physics A*, **66**, S397–S402, (1998).

[52] P.W. Kolb, *Private Communication*.

[53] C. Durkan and I. V. Shvets, "Reflection-mode scanning near-field optical microscopy: Influence of sample type, tip shape, and polarization of light," *Journal of Applied Physics* **83,** 1171 (1998).

[54] K. D. Weston, J. A. DeAro, and S. K. Buratto, "Near-field scanning optical microscopy in reflection: A study of far-field collection geometry effects," *Review of Scientific Instruments* **67,** 2924, (1996).

[55] C. Durkan and I. V. Shvets, "Polarization effects in reflection-mode scanning near-field optical microscopy," *Journal of Applied Physics* **83,** 1837, (1998).

[56] N. F. Vanhulst, F.B.Fegerink, B Bolger "High-resolution Imaging of Dielectric Surfaces with an Evanescent Field Optical Microscope" *Optics Communications* **87**, 212, (1992).

[57] Christian Girard, Alain Dereux, Olivier J. F. Martin, Michel Devel, "Generation of Optical Standing Waves around Mesoscopic Surface Structures: Scattering and Light Confinement," *Physical Review. B* **52**, 2889, (1995).